ICEMG 2023-XXXXX

Dual Stator Electric Machine Equipped with Permanent Magnets on Both Stators for Electric Vehicles

Arash Mousaei

Factually of Electrical and Computer Engineering University of Tabriz, Tabriz; a.mousaei@tabrizu.ac.ir

Abstract

A new type of Dual Stator Permanent Magnet (DSPM) machine, which is capable of producing high torque at low operating speed, for direct-drive applications is proposed and analyzed in this study. ANSYS-MAXWELL-2D/3D computational software is employed in the prediction of the machine performances, using the finite element technique. The considered machine performance indices are flux linkage, Electromotive Force (EMF), inductances, torque, losses, and efficiency. It is found that the proposed machine has better output torque performance than its single stator equivalent; though, with attendant higher cost and manufacturing complexity. Moreso, the proposed machine has sinusoidal and symmetrical flux linkage and electromotive force waveforms. These qualities are desirable for smooth control operations of brushless Alternating Current (AC) machines; and direct-drive uses. Further, the impact of design parameters on the performance of the proposed DSPM machine is also considered in this work. The investigated geometric design variables include the: split ratio (S_o), Permanent Magnet (PM) size, rotor radial thickness (R_t), stator tooth thickness (W_t), rotor inner iron-width/pitch ratio (R_{iw}), and rotor outer iron-width/pitch ratio (R_{ow}), etc. The overall machine model is obtained using the intrinsic evolutionary optimization algorithm of the adopted software.

Keywords: Electric Vehicle, Dual stator, electromotive force, flux linkage, losses, and structural variables.

Introduction

High-torque permanent magnet machines are desirable in low-speed direct-drive applications, such as in-wheel vehicle uses. Consequent to this, a lot of researchers are currently directing attention toward such kinds of machines. Therefore, a dual stator permanent magnet (DSPM) machine that belongs to the flux-switching machine class and is suitable for low-speed and high-torque direct-drive operations is proposed and investigated in this present study.

Vernier permanent magnet (VPM) machines having dual-stator structure and different topologies are introduced in [1] and [2], to enhance the usual low power factor characteristics of VPM machines. The inner stator areas are fully equipped with distributed windings in both machine types presented in [1] and [2]. Hence, this kind of winding arrangement aids the generated air-gap flux density level of these machines; nevertheless, with increased cost and reduced the machine's overall efficiency compared to an equivalent machine that has a concentrated winding configuration. It is worth mentioning that a non-overlapping concentrated winding configuration is applied in this current study. More so, the enhanced power factor in [2] is realized by adjusting the relative position between the inner and outer stator poles, in addition to the deployment of spoke-array kind of permanent magnets (PMs) orientation, for better flux concentration around the air-gap. However, at a high-cost penalty, owing to the increased volume of magnets consumed in such a machine, despite the natural high flux leakages that are associated with VPM machines.

Further, dual stator permanent magnet machines are recommended in [3] and [4]; though, the recommended machines have weak structural strengths. The recommended dual stator machines would also generate a high amount of eddy current loss; owing to the location of magnets on the rotor part. This high eddy current loss flaw would be aggravated at high operating speed and loading conditions, which would eventually affect the machine's overall efficiency.

Furthermore, a double stator permanent magnet machine with improved thermal and torque capabilities is proposed in [5]. However, the investigated machine in [5] has low resultant flux linkage between the stators via the rotor. Also, the required magnetic field modulation influence is less effective, coupled with the poor magnet retention problem in the machine, due to its structural design that could cause further mechanical issues, especially at high working speed.

Meanwhile, the impact of combining the right stator and rotor pole numbers of a given permanent magnet machine, as well as the appropriate use of its optimized geometric variables are highlighted in [6], with a view to yielding the required good overall machine performance. The declaration about the critical roles of optimal geometric dimensions in electrical machines is demonstrated in [7] and reconfirmed in [8]; where it is ascertained that the overall electromagnetic performance of an electric machine would largely depend on values of its optimal structural geometric variables. Although, the analyzed machine in [7] may yield reasonable power factor and torque density compared to other conventional double stator permanent magnet machines; it would have more fabrication complications, owing to the irregular sizes and pole arcs of the used magnets.

It is revealed in [9] that by doubling the stator segment of a dual-stator switched-flux PM machine having an even number of rotor poles; then, its induced-electromotive force, output torque and efficiency values would be greatly improved. Additionally, the machine's undesirable elements such as total harmonic distortion, cogging torque, and torque ripple would be drastically reduced compared to that of the conventional single stator switched-flux machine type; however, with heavier machine weight and high-cost consequence. By extension, the proposed machine in [9] would most likely offer a longer life span to the system due to its negligible noise and vibration properties, since the machine would be free of unbalanced magnetic force by the nature of the machine’s doubled even pole number. Generally, double-stator electric machines usually have higher output performance than their equivalent single-stator counterparts [10]; albeit, with increased manufacturing complexity and cost implications.

Similarly, a double stator PM machine that is capable of providing an extended speed range, as well as improved flux controllability, is proposed in [11]; the enhanced flux regulation perspective is achieved by furnishing the inner stator with field windings. However, the rotor of the analyzed machine in [11] is equipped with permanent magnets which may increase the level of eddy current loss in the machine; specifically, at high operating speed and temperature, in addition to the poor reliability and reduced fault tolerance ability of such machine, due to the magnetic flux cross-coupling interactions between the armature coils and field coils. Nevertheless, the fault-tolerant potential of a given double stator PM machine could be improved by modifying the slot opening size of the machine, as recommended in [12]. It is claimed in [12] that by this slot opening special adjustment; then, the self-inductance of the machine would be boosted with a corresponding low ratio of mutual inductance to self-inductance outcome. Note that this low inductance ratio is an admirable fault-tolerance feature; notwithstanding, the recommended machine has a complicated rotor structure.

In this current study, a new type of high performance low speed permanent magnet machine having a two-stator structure is proposed, for potential implementation in direct drive applications. The sections of this investigation are organized as follows: The background of the study is presented in Section 1. The working principle of the proposed machine, its materials, and the adopted methodology is presented in Section 2. The influence of the machine’s structural dimensions is provided in Section 3. The results are discussed in Section 4, while the conclusion is given in Section 5.

Materials and Method

The implemented core and permanent magnet materials in this work are listed in Table 1. Note that the proposed dual stator machine is conceived from the single-stator flux-switching permanent magnet machine (SS-FSPMM); however, it has a more complicated architectural plan than the SS-FSPMM, and that would also entail higher manufacturing costs. The diagram of the conventional SS-FSPMM and the proposed DSPM machine model is displayed in Figure 1 (a) and (b), respectively. A+ and A-, B+ and B-, and C+ and C- are the Phase A, Phase B, and Phase C coil sides, respectively.

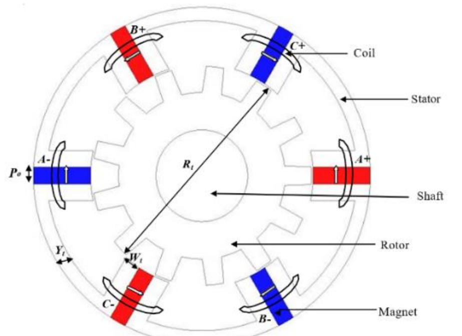

(a) Original PM machine i.e., SS-FSPMM [13]

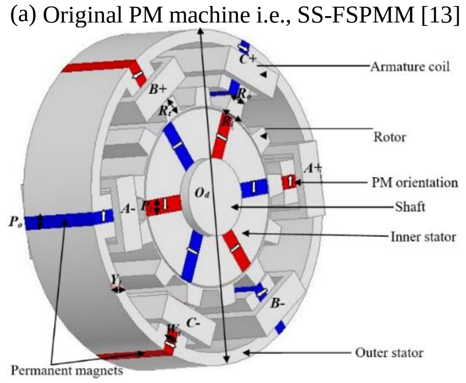

(b) 3D-FEA model of the proposed machine

Figure 1. The investigated machine structures

Each set of permanent magnets (PMs) in the separate stators are arranged such that each permanent magnet (PM) would have an opposite magnetization path with its adjacent magnet. In addition, the PMs in the inner stator must have opposite polarities from the corresponding ones in the outer stator, to produce the required electromagnetic torque. Moreover, the adopted spoke an array of magnets in this study is essential for improved air-gap flux density. The rotor which is positioned between the stators serves as a field-modulating component and it is made of steel pieces in a ring form. It is worth noting that the rotor pieces are joined together using steel material of 0.5 mm width. Also, the shaft is made of non-magnetic steel material. Practically, the rotor would be supported mechanically by non-magnetic rods enclosed in a shell made of epoxy material. In practice, the front side of the rotor is designed such that it would rest upon a bearing positioned at the interior part of the machine’s cover plate, while the other end of the rotor is sited on another bearing, mounted on the shaft. Moreover, a combination of an external fan and natural air-cooling method is recommended for the effective thermal management of the proposed machine, considering its small size of 45 mm outer radius. The forced external air could be applied through perforations/bores of the machine’s non-magnetic steel casing. Nevertheless, an enlarger size machine would require a special cooling mechanism.

Description of the proposed machine’s operating principle is narrated as follows: When the machine is energized by a three-phase sinusoidal current, it will produce a flux linkage which will in turn induce an electromotive force (EMF) on the windings and subsequently generate the machine’s output torque. It is worth noting that the proposed machine when functioning under open circuit conditions, records its least negative flux linkage value on Phase A coils. This least negative flux linkage value occurs when the rotor is still at the zero electrical angular position, and this corresponds to the machine's negative direct-axis point. On rotating the rotor forward by 90 degrees electrical shift, then, the resultant flux linkage amplitude would be zero, and this position coincides with the quadrature-axis locus of the machine. Further, when the rotor moves 180 electrical degrees from the initial rotor position; then, the resultant flux linkage would attain its largest positive value. This new position denotes its positive direct-axis position. At a 270 electrical degrees rotation from the initial rotor position, the machine would obtain another zero resulting flux linkage value; this position is also the quadrature-axis position of the rotor, though, in the reverse direction. Also, when the rotor moves forward to 360 electrical degrees from its start point, which corresponds to one electrical revolution; the resulting flux linkage would have peak negative magnitude i.e., another negative least value. Overall, the resulting flux linkage would yield a bipolar waveform which is a desired feature for efficient electric machine control operations. A clearer picture of the above operating scenarios is represented in Figure 2, using magnetic flux line contours. Note that rate of change of the produced flux linkage with respect to time, will yield the required EMF on the armature windings, and consequently result in torque generation.

Due to the twofold operating feature of the proposed machine i.e., its flux-switching and flux-modulation mode of operations; it is classified as both a flux-switching PM machine and a magnetically-geared PM machine. The flux-switching action of the machine is essentially its capability to reverse its magnetic flux linkage path within one electric revolution; thereby, generating a bipolar flux-linkage waveform and a corresponding bipolar EMF waveform. Meanwhile, the machine's ability to modulate its effective air-gap flux density emanating from both the armature windings and magnets, with the help of modulating ring (i.e., the rotor in this present case), in order to produce an output torque, is termed the magnetic-gearing effect. Refined tiny and discrete mesh elements are applied in the whole simulation model, in order to ensure a high level of precision in the obtained FEA results. Magnetic flux outlines of the proposed machine are displayed in Figure 2.

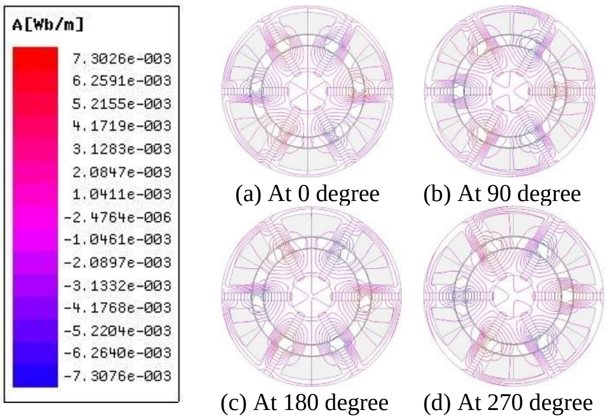

(a) At 0 degree (b) At 90 degree

(c) At 180 degree (d) At 270 degree

Figure 2. Flux lines of the proposed machine on no-load, 2D-FEA

Furthermore, the machine's structural dimensions are obtained through an inherent evolutionary optimization procedure, embedded in the implemented software. The machine's dimensions and applied materials are listed in Table 1. The stator phase resistance is stated in equation (1). Under the implemented genetic algorithm optimization approach, all the leading design parameters enumerated in Table 2, are optimized simultaneously. Note that there could be noticeable differences in the optimal values of geometric parameters obtained through individual parametric optimization and its equivalent global optimization via the genetic algorithm, as reported in [14]. Global optimization procedure usually yields improved results compared to that individual parametric optimization. Similarly, the adopted genetic algorithm is computed at a constant copper loss value of 30W, while considering other factors such as the machine's geometric limits, population size, regeneration, mutation and target weight, etc. as provided in Table 2. The implemented linear optimization cost function (C) of the genetic algorithm is mathematically stated in equation (2). Meanwhile, the copper loss (P_{cu}) relation is given in equation (3). Also, the pitch ratio (α_r) is specified in equation (4). More so, the adopted genetic algorithm setup and flow chart are displayed in Figure 3.

$$R_{\emptyset} = \frac{2\rho_{20} L_a N_c n_t}{k_w A_s} \tag{1}$$

Where: L_a is the machine's stack length, N_c is the number of coils per phase, n_t is the number of turns per coil, k_w is the winding factor, ρ_{20} is the resistivity of copper at an operating temperature of 20°C, and A_s is the slot area per coil side. End winding length is neglected in this estimation.

$$C = -\sum_{m=1}^{N} |T_w W_m| \tag{2}$$

Where: C, N, T_m, and W_m are the cost function, number of iterations, target mean torque, and the weighted target value, respectively. Note that the set objective or goal is equal to the largest mean torque (T_{avg}).

$$P_{cu} = 3I_{rms}^2 R_{\emptyset} \tag{3}$$

Where: I_{rms} is the root mean square current, R_{ϕ} is the stator phase resistance.

$$\alpha_r = \frac{360^{\circ}}{P_r} \tag{4}$$

Where: P_r is the rotor pole number.

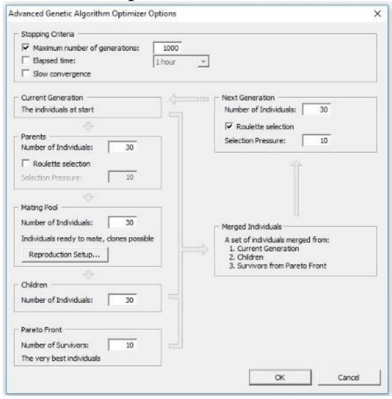

Figure 3. FEA extracted the genetic algorithm setup and flowchart [15]

Table 1: Elements of the investigated machines

Item	Value	
Stator pole number	6	
Rotor pole number	13	
Air-gap length, mm	0.5	
Stack length (La), mm	25	
Machine outer radius (Od), mm	45	
Winding factor (kw)	0.6	
Steel material	M330–35A	
Conductor material	Copper	
Magnet material	N35SH	
Number of turns/phase	72	
DC link voltage (Vdc), V	36	
PM remanence (Br), T	1.2	
Operating temperature, oC	20	
Number of turns per coil (nt)	36	
Number of coils per phase (Nc)	2	
Operating speed, rpm	400	
Rated current, A	15	
Coercivity (H), A/m	-909456.8177	
Comparison	**SS-FSPMM**	**Proposed DSPM machine**
Outer stator PM thickness (P_o), mm	4.45	3.4
Inner stator PM thickness (P_i), mm	Not applicable	4.03
Rotor radial size (R_t), mm	29.25	5.296
Slot area per coil side (A_s), mm^2	278.86	294.42
Outer stator tooth-thickness (W_t), mm	4.4	4.15
Rotor inner iron-width / pitch ratio (R_{iw})	Not applicable	0.55
Rotor outer iron-width / pitch ratio (R_{ow})	Not applicable	0.35
Stator yoke thickness (Y_t), mm	3.6	3.44
Split ratio (S_o)	0.65	0.66
Magnet volume, mm^3	10175.8	15745.4

The split ratio (S_o) of the analyzed machine is given as the ratio of the machine's effective air-gap length to that of the machine's outer span, as expressed in equation (5). Also, the mathematical expression of the rotor inner iron-width/pitch ratio (R_{iw}) and rotor outer iron-width/pitch ratio (R_{ow}) is given in equations (6) and (7), respectively.

$$S_o = \frac{A_{gl}}{O_d} \tag{6}$$

Where: A_{gl} is the length of the working air gap and O_d is the outer span of the machine.

$$R_{iw} = \frac{R_i}{\alpha_r} \tag{7}$$

$$R_{ow} = \frac{R_o}{\alpha_r} \tag{8}$$

Where: R_i and R_o are the rotor inner iron-width and rotor outer iron-width.

Influence of the Machine Structural Dimensions

This section is dedicated to the influence of machine structural or geometric dimensions/variables on the performance of the proposed DSPM machine, using two- dimensional finite element analysis (2D-FEA) method. It is worth noting that each parameter is scanned independently in this section of the study, using individual parametric optimization techniques. The output of an electrical machine is directly related to its varying structural dimensions. More importantly, the influence of the split ratio on the overall machine performance is usually significant, because it is linked to the machine's total size. Although, structural dimensions of electrical machines could be estimated faster using analytical/modeling techniques, as demonstrated in [15]; however, analytical procedures usually fall short of high precision accuracy, due to their inherent numerous modeling assumptions, compared to the implemented finite element analysis (FEA) approach, in this current study. The report in [16] shows that an electric machine that has an optimal split ratio, would deliver better output electromagnetic performances; since the split ratio is critical in determining the machine's overall productivity.

Table 2: Optimization parameters, constraints and settings

Parameters	**Value**		
	Sensitivity range	**Initial value**	**Optimum value**
Split ratio (S_o)	[0.5–0.8]	0.4	0.66
Outer stator PM thickness (P_o), mm	[2–5.5]	2.5	3.4
Inner stator PM thickness (P_i), mm	[2–5.5]	2.5	4.03
Rotor radial size (R_r), mm	[3–6]	3	5.296
Outer stator tooth-thickness, (W_t), mm	[2–5]	3	4.15
Rotor inner iron-width / pitch ratio (R_{iw})	[0.1–0.9]	0.2	0.55
Rotor outer iron-width / pitch ratio (R_{ow})	[0.1–0.9]	0.2	0.35
Stator yoke thickness (Y_t), mm	[2–5]	3	3.44
Fixed copper loss, W	30		
Peak flux density, T	1.2		
Crossover type	simulated binary		
Individual crossover likelihood	0.5		
Variable crossover likelihood	0.5		
Standard deviation	0.05		
Mutation type	polynomial		
Set goal	1		
Target weight (W_m)	1		

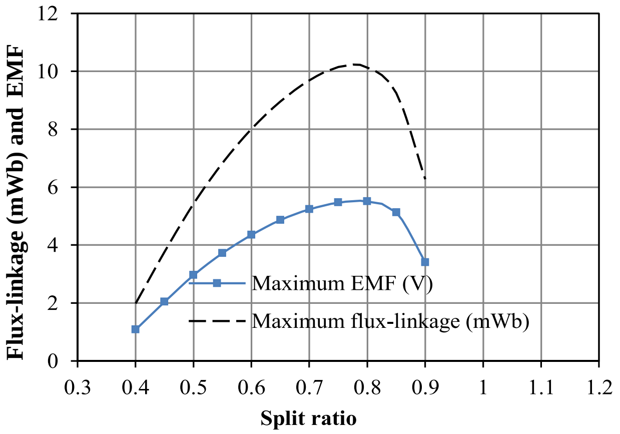

(a)

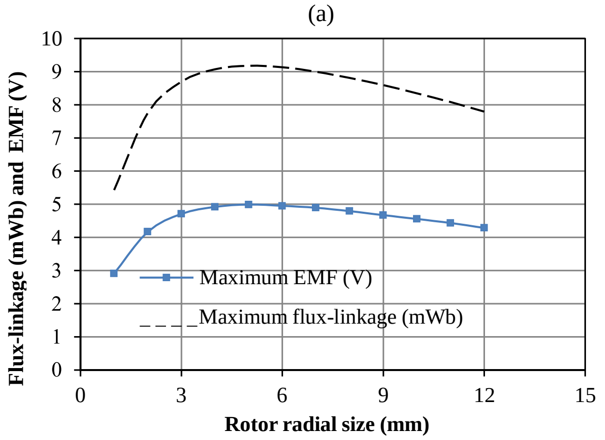

(b)

Figure 4. Comparison of flux linkage and EMF with: a) split ratio, and b) rotor radial size

Figure 4(a) shows the variation of the split ratio with flux linkage and induced- electromotive. The rise and fall of the output values shown in Figure 4(a) is a direct consequence of the amount of electric loading in the machine, resulting from the available coil spaces, due to the varying split ratio. It is worth noting that the performance of a typical flux-switching permanent magnet machine is largely determined by its split ratio value, as proved in [17].

Similarly, when the rotor radial size is very small, it would result in high magnetic saturation of the concerned region (s) and consequently reduced output performance. However, when the rotor radial size is excessively large, then, it would create an opportunity for high leakage fluxes, which will again reduce the overall output performance of the machine. Therefore, a balance between these extreme conditions is essential in order to yield the optimum rotor size value, which is about 5 mm in this case, as shown in Figure 4(b). Note that there will be no output flux linkage and EMF when the rotor radial size is abridged to a zero value. Also, Figure 5 shows the variation of flux linkage and EMF with both the inner and outer stator PM widths. The initial increase in PM thickness would result in an enhanced PM flux linkage; however, an enlarged PM thickness would also have a negative effect on the space availability in the slots, for the excitation windings. This reduction in the available space would result in reduced machine performance. The optimum value of the PM thickness is approximately 4 mm.

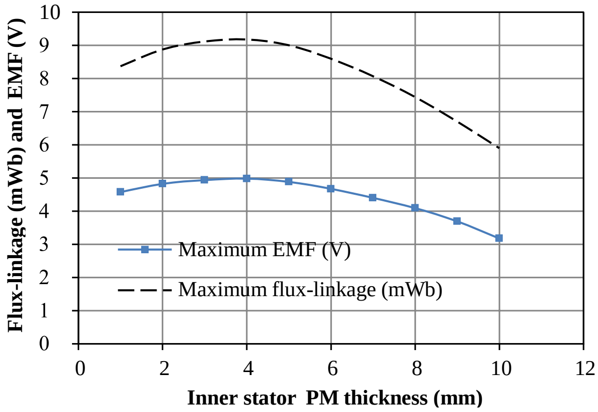

(a)

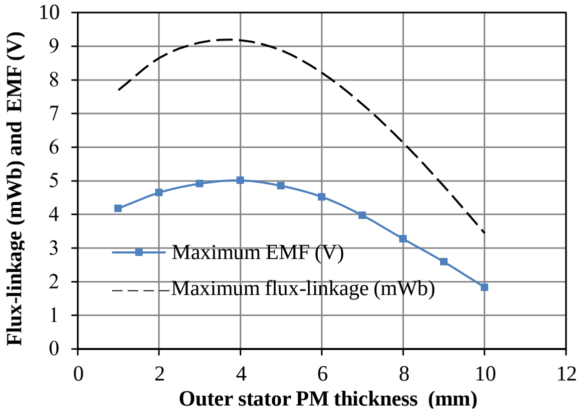

(b)

Figure 5. Comparison of flux linkage and EMF with PM thickness: a) Inner stator permanent magnet thickness (mm), and b) Outer stator permanent magnet thickness (mm)

Figure 6(a) depicts the variation of outer stator tooth-width or thickness with the resulting flux linkage and EMF values; the output performances are seen to be very sensitive to the stator tooth-thickness. Oversized tooth-width would result in lower machine outputs, owing to the reduced applied phase current, which is dependent on the available slot areas, at fixed copper loss conditions. Meanwhile, the very small size of the stator tooth-width would also lead to lower machine overall performance, due to the electromagnetic saturation effect caused by the armature reactions. It could be observed from Figure 6(b) that the flux linkage and EMF values of the investigated machine rise first with increasing back-iron thickness up to about 3 mm, and then, becomes insensitive to the progressively varying back-iron thickness, due to high level of flux leakages under such condition.

The optimal values of the rotor inner iron-width/pitch ratio (R_{iw}) and rotor outer iron-width/pitch ratio (R_{ow}) are 0.6 and 0.35, respectively, as shown in Figure 7. The resulting values of these two parameters would rely on the ensuing flux linkages around the rotor pole arcs/widths of the machine, owing to its possible electromagnetic loading, at any particular time.

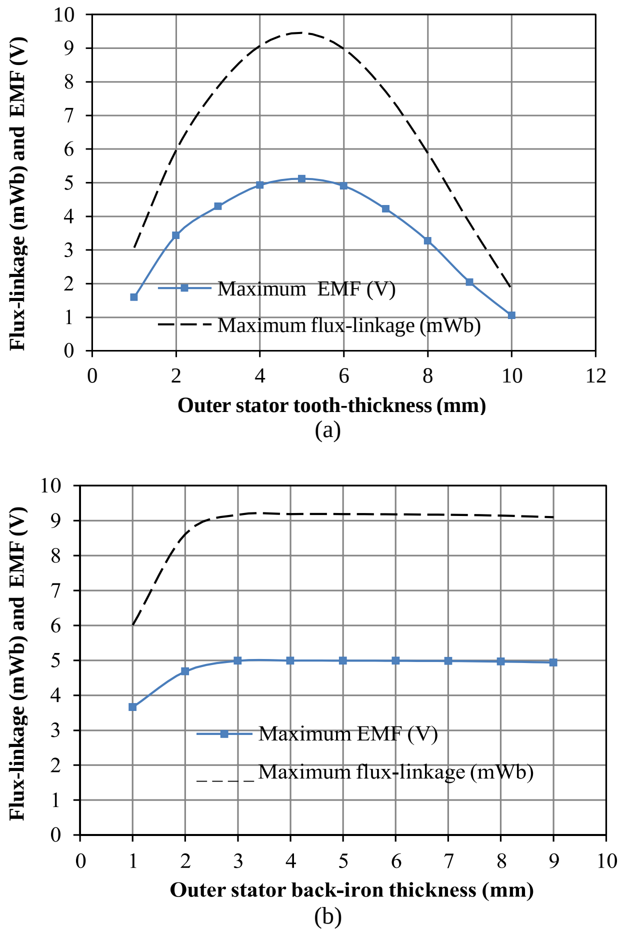

Figure 6. Comparison of flux linkage and EMF with PM thickness: a) Outer stator tooth-thickness (mm), and b) Outer stator back-iron thickness (mm)

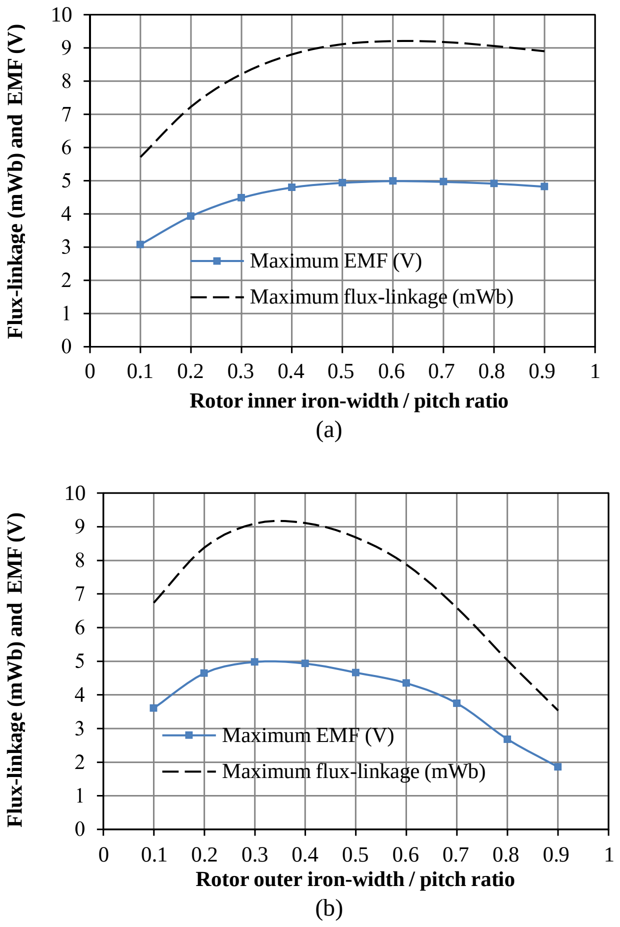

Figure 7. Comparison of flux linkage and EMF with PM thickness: a) Rotor inner iron-width/pitch ratio (mm), and b) Rotor outer iron width/pitch ratio (mm)

Results and Discussions

Figure 8 shows the no-load torque comparison of the investigated machines. It is observed that the cogging torque amplitude of the DSPM machine and its original PM machine counterpart is 0.145 Nm and 0.028 Nm, respectively. These cogging torque magnitudes are not significant, because it is only about 5 % of the output torque. Cogging torque cycles (T_c) in one electrical revolution are expressed in equation (8). Thus, for a 13-rotor pole machine having 6 stator slots, equation (8) will yield 6 cycles as realized in Figure 8.

$$T_c = \frac{LCF(P_r, S_{th})}{P_r} \quad (8)$$

Where: LCF is the lowest common factor between stator and rotor pole numbers, P_r and S_{th} are the rotor pole number, and combined stator teeth number [18].

Similarly, the coil and phase flux linkages and EMFs of the analyzed DSPM machine are depicted in Figures 9 and 10. It is shown that the flux linkage and EMF waveforms are symmetrical and sinusoidal in shape, and this is necessary for efficient electric machine control. It is also revealed that the separate coils per phase make equal contributions to the overall flux linkage and induced EMF values. It is worth noting that there is 8.4% difference between the compared 2D-FEA and 3D-FEA phase flux-linkage amplitudes shown in Figure 8, this is as a result of the impact of the end windings.

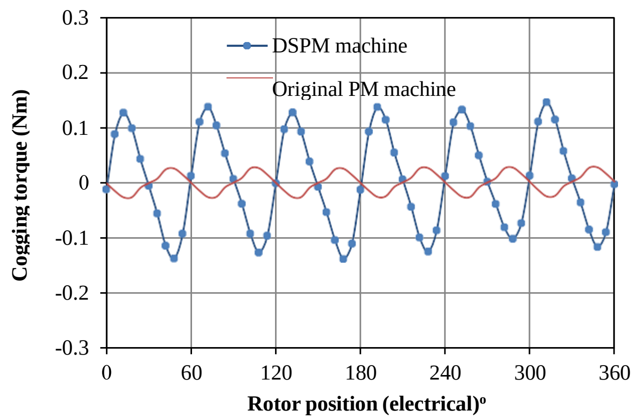

Figure 8. Comparison cogging torque versus rotor position, 2D-FEA

The variation of flux linkage, EMF, and average torque with rotor speed current are shown in Figure 11. It is observed that the EMF value is dependent on both the rotational speed and the applied current, as displayed in Figure 11(b); while the flux linkage and average torque values are proportional to the supplied current, though, both the flux linkage and average torque values have an insensitive response to change in rotational speed, as presented in Figure 11(a) and (c).

The static torque waveforms of the investigated DSPM machine shown in Figure 12, show the machine's performance-reliance on the supplied amount of current, i.e., the higher the input current, then, the larger its static torque magnitude. Similarly, the electromagnetic torque waveform of the proposed machine is shown in Figure 13(a). It is observed that there is about 9.9% difference between the predicted 2D-FEA and 3D-FEA electromagnetic torques of the proposed DSPM machine. Moreover, the torque-speed and power-speed curves of the proposed DSPM machine are shown in Figure 13(b). The peak torque and power of the proposed machine operated at a maximum current (I_{max}) of 15 A and maximum voltage (V_{max}) of 22.9 V is 2.63 Nm and 508.72 W, respectively. Note that the maximum field-weakening speed of the investigated DSPM machine is 6800 rpm. The estimated maximum inverter voltage is given in equation (9).

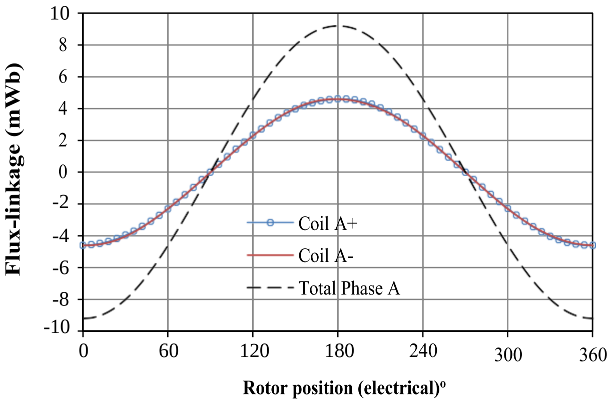

(a)

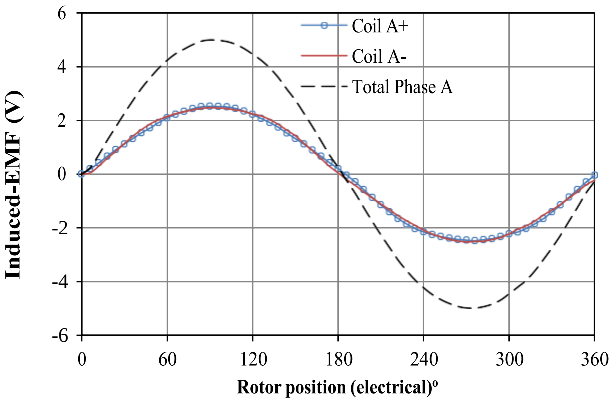

(b)

Figure 9. Comparison of flux linkage and EMF waveforms at 400 rpm, 2D-FEA: a) Flux linkage versus rotor position, and b) Electromotive force versus rotor position

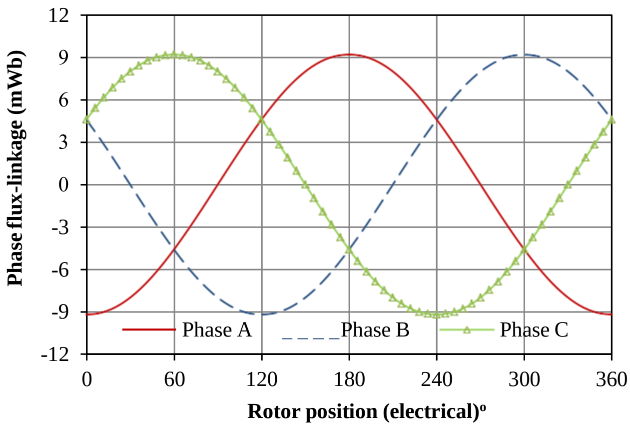

(a)

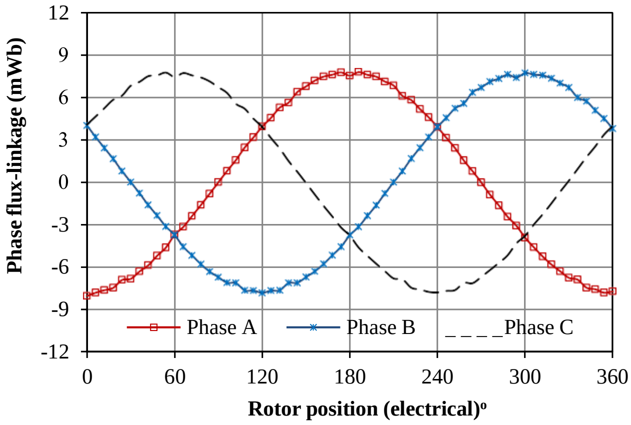

(b)

Figure 10. Comparison of flux linkage waveforms at 400 rpm: a) Three-phase flux linkage, 2D-FEA, and b) Three-phase flux linkage, 3D-FEA

$$V_{max} = \frac{2 \times V_{dc}}{\pi} \tag{9}$$

Where: V_{dc} is the direct-current link voltage.

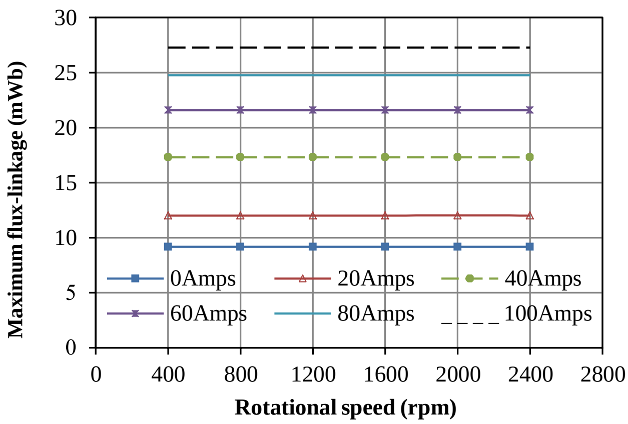

(a)

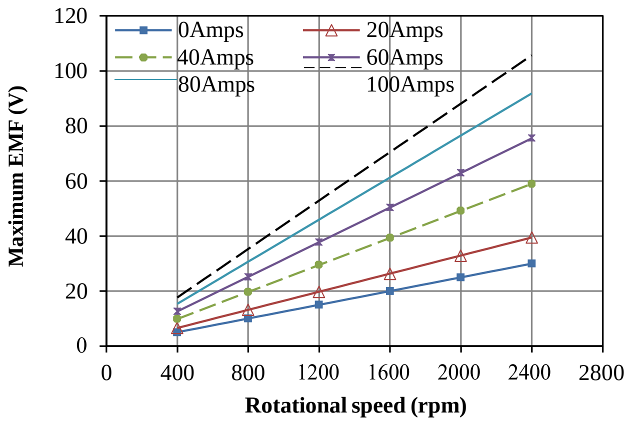

(b)

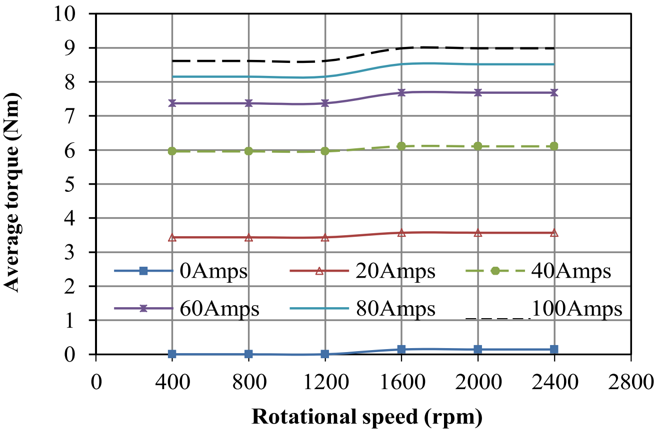

(c)

Figure 11. Comparison of flux linkage, EMF and torque with load current and rotor speed, 2D-FEA: a) (a) Flux linkage versus speed, b) EMF versus speed, and c) Average torque versus speed

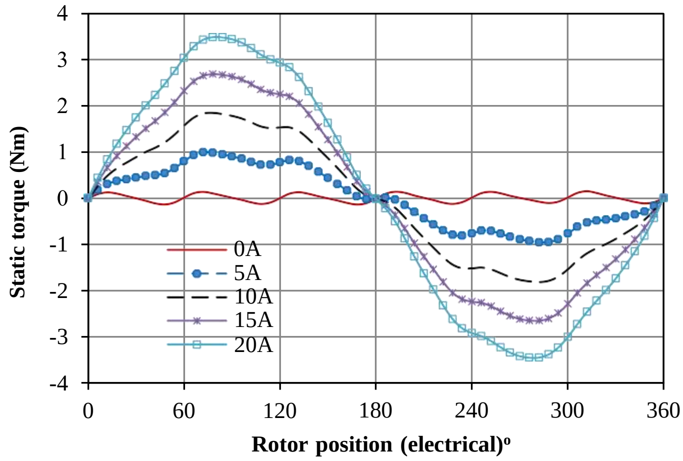

Figure 12. Comparison of static torque with rotor angular positions, 2D-FEA

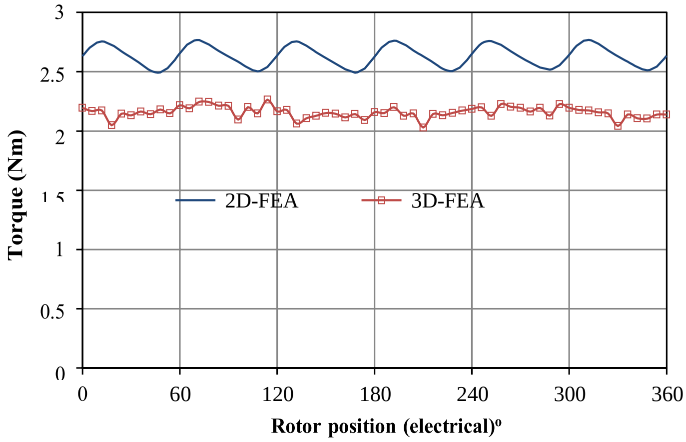

(a)

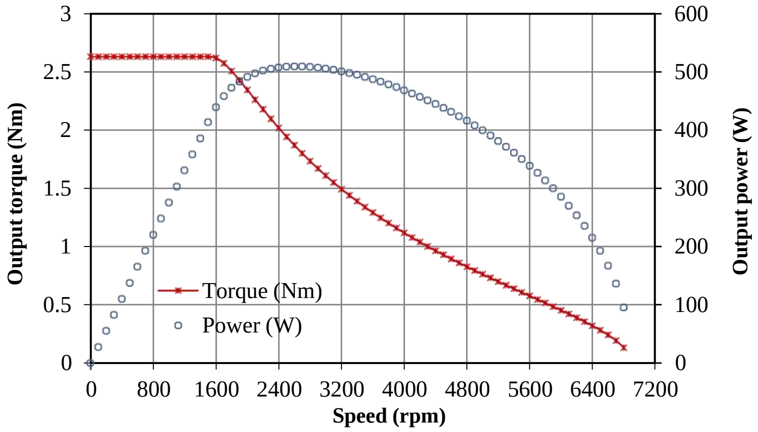

(b)

Figure 13. Output torque and power versus rotor speed at 15 A, V_{dc}=36 V: a) Torque versus rotor position, and b) Torque versus speed

Similarly, the variation of average torque with current density and copper loss depicted in Figure 14, presents the DSPM machine as a better candidate than its single stator counterpart; particularly, with respect to its withstand capacity to saturation effects caused by electric loads. Hence, the DSPM machine would have higher overload withstand potential than the original PM machine i.e., the SS-SFPMM. This justifies the notion in [18] that the performance of a double-stator machine exceeds that of its single-stator equivalent.

The self-inductance and mutual-inductance outlines of the compared machines are presented in Figure 15. It is observed that the original PM machine has both higher self-inductance and mutual inductance values, relative to the DSPM machine. This feature is a good lower mutual inductance as well as the lower absolute ratio of mutual inductance to self-inductance, compared to the original PM machine. These low mutual inductance characteristics are necessary for higher reliability and improved fault-tolerance ability of a given electric machine, as highlighted in [17]. It also implies that the proposed DSPM machine has higher magnetic isolation between the phase windings, possibly due to its larger slot area, owing to the differences in their respective split ratios, as provided in Table 1. The predicted 3D-FEA inductance values are higher than their corresponding 2D-FEA counterparts, due to the influence of end windings. Also, the negative mutual inductance values depict reverse current directions in the adopted phase winding polarities. The compared 2D-FEA and 3D-FEA inductance values of the investigated machines are listed in Table 3.

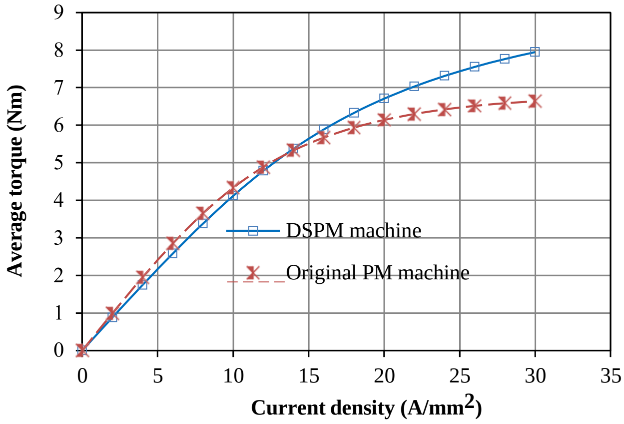

(a)

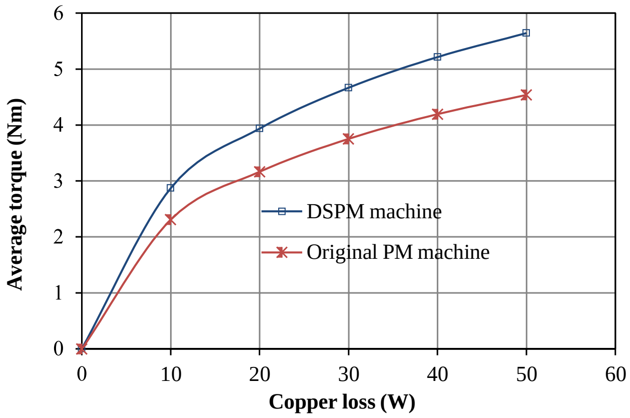

(b)

Figure 14. Comparison of average torque with current density and copper loss, 2D-FEA: a) Average torque versus current density, and b) Average torque versus copper loss

The self-inductance and mutual-inductance outlines of the compared machines are presented in Figure 15. It is observed that the original PM machine has both higher self-inductance and mutual inductance values, relative to the DSPM machine. This feature is a good lower mutual inductance as well as the lower absolute ratio of mutual inductance to self-inductance, compared to the original PM machine. These low mutual inductance characteristics are necessary for higher reliability and improved fault-tolerance ability of a given electric machine, as highlighted in [18]. It also implies that the proposed DSPM machine has higher magnetic isolation between the phase windings, possibly due to its larger slot area, owing to the differences in their respective split ratios, as provided in Table 1. The predicted 3D-FEA inductance values are higher than their corresponding 2D-FEA counterparts, due to the influence of end windings. Also, the negative mutual inductance values depict reverse current directions in the adopted phase winding polarities. The compared 2D-FEA and 3D-FEA inductance values of the investigated machines are listed in Table 3.

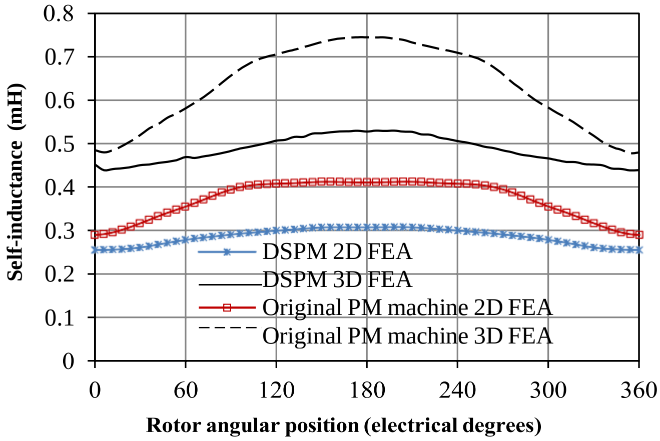

(a)

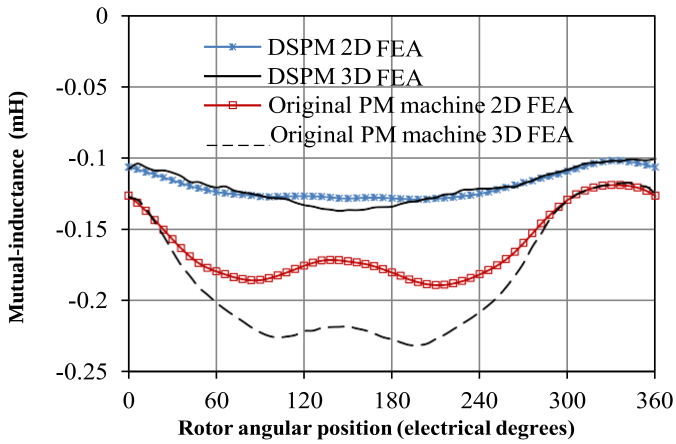

(b)

Figure 15. Comparison of self- and mutual-inductances, 2D/3D-FEA: a) Self-inductance, and b) Mutual-inductance

The self-inductance (L_{aa}) and mutual-inductance (M_{ab}) of the compared machines are estimated using equations (10) and (11).

$$L_{aa} = \frac{\varphi_{P-Ia} - \varphi_p}{I_a} \tag{11}$$

$$M_{ab} = \frac{\varphi_{P-Ib} - \varphi_p}{I_a} \tag{12}$$

Where: I_a is the supplied peak current in phase A, Φ_{p_Ia} is the flux linkage contribution in Phase A by the PMs and the excited windings of phase A, Φ_{p_Ib} is the flux linkage contribution in Phase B by the PMs and the excited windings of Phase A and Φ_p is the flux linkage contribution by the PMs only on open circuit situation.

Table 3: Comparison of 2D-FEA and 3D-FEA inductances

Item	Value			
Type of Machine	DSPM Machine	Original PM Machine	DSPM Machine	Original PM machine
Finite Element Analysis	2D FEA		3D FEA	

Peak self-inductance, mH	0.3080	0.4111	0.5296	0.7450
Average self-inductance (L_{aa}), mH	0.2862	0.3706	0.4848	0.6329
Peak mutual inductance, mH	-0.1020	-0.1192	-0.1007	-0.1177
Average mutual-inductance (M_{ab}), mH	-0.1199	-0.1626	-0.1199	-0.1856
The absolute ratio of M_{ab} to L_{aa} (%)	41.88	43.85	24.74	29.33

Figures 16(a) and (b) show the comparison of magnet eddy current loss and total core loss variations with the rotational speed, of the investigated machines. It could be inferred that the DSPM machine possesses higher amount of magnet eddy current loss owing to its larger amount of PM volume; albeit, with a lower total core loss amount. More so, the resultant efficiency of the proposed DSPM machine is higher than that of the original PM machine, due to its better output torque and lower overall loss value. Figure 16(c) compares the efficiencies of the analyzed machines with respect to the machine's rotational speed. The predicted core loss of the machine is calculated using equation (12).

$$W = W_h + W_e + W_a = \left[k_h B_{max}^2 f + \sigma \frac{q^2}{12} (\frac{dy}{dx}(t))^2 + k_a (\frac{dy}{dx}(t))^2\right] k_s \quad (13)$$

Where, W_h, W_e, W_a are the hysteresis, eddy current and anomalous losses, respectively; f, B_{max}, q are the operating frequency, peak flux-density, sheet width, respectively; k_h, k_a, k_s and σ are the hysteresis, anomalous, conductor stacking constants, and core material conductivity coefficient [21].

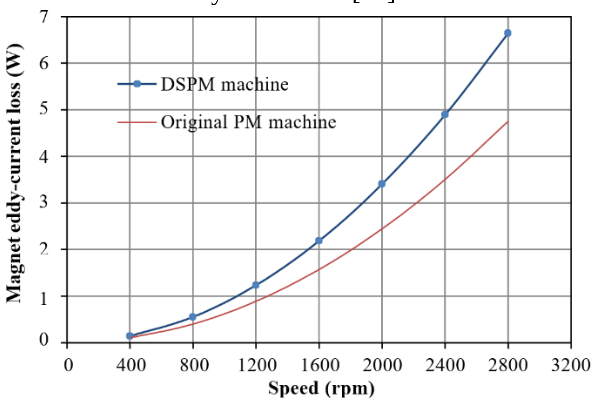

(a)

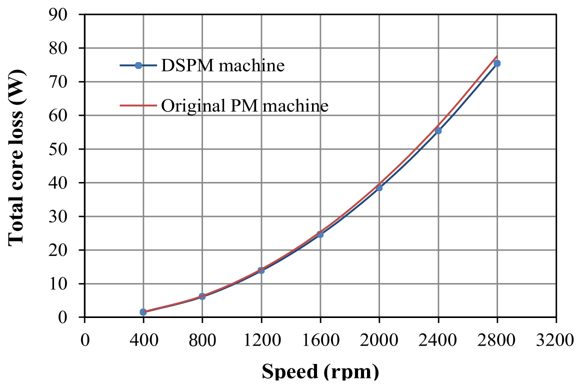

(b)

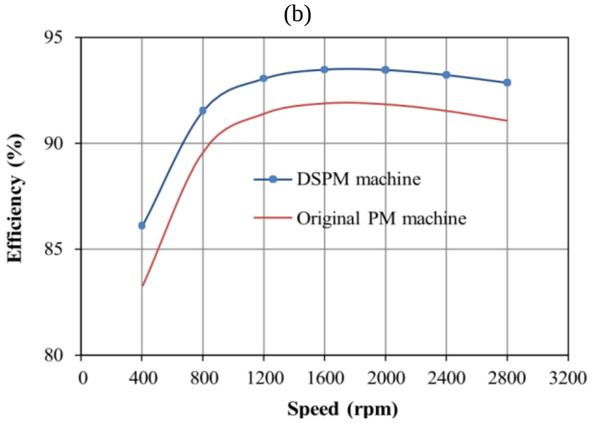

(c)

Figure 16. Comparison of losses and efficiency at 15A, 2D-FEA: a) Eddy current loss versus speed, b) Total core loss versus speed, and c) Efficiency versus speed

Conclusion

A new type of dual stator permanent magnet (DSPM) machine suitable for low-speed high torque direct drive in-wheel applications is proposed and presented. The efficiency of the proposed machine outweighs that of the original PM machine; though, with greater amount of PM eddy current loss and possible higher manufacturing cost and complexity. Moreover, the overload-withstand potential of the DSPM machine is much higher than of the compared single stator type. Additionally, the proposed DSPM machine would exhibit higher magnetic isolation between its windings and lower mutual-inductance to self-inductance ratio; and this implies, improved fault-tolerance capability, though, with a lower short-circuit withstand proficiency, compared to its single stator equivalent. The investigation also shows that the output of the proposed DSPM machine would be dependent upon the model's structural dimensions/sizes. Hence, there is need to apply the optimum machine dimensions, in order to achieve the best machine performance. In addition, most of the machine's performances are shown to be a function of its operating speed and the applied current.

References

[1] F. Zhao, T.A. Lipo and B.I. Kwon, "Dual-stator interior permanent magnet vernier machine having torque density and power factor improvement," Electric Power Components and Systems, vol. 42,

no. 15, pp. 1717–1726, 2014. DOI: 10.1080/15325008.2014.950360.

[2] D. Li, R. Qu and T.A. Lipo, “High-power-factor vernier permanent-magnet machines,” IEEE Transactions on Industry Applications, vol. 50, no. 6, pp. 3664–3674, Nov./Dec. 2014. DOI: 10.1109/TIA.2014.2315443.

[3] J.H. Park, G.F. Lukman, D.H. Kang and J.W. Ahn, “Performance characteristics of a dual-stator, spoke-type permanent magnet vernier machine with support bar,” Energies, vol.14,no.4,pp. 1068 ,Feb. 2021. DOI: 10.3390/en14041068.

[4] A. Mousaei and M. B. B. Sharifian, "Design and optimization of a linear induction motor with hybrid secondary for textile applications," 2020 28th Iranian Conference on Electrical Engineering (ICEE), 2020, pp. 1-6, doi: 10.1109/ICEE50131.2020.9260773.

[5] M.R. Siddiqi, T. Yazdan, J.H. Im, M. Humza and J. Hur, “Design and analysis of a dual airgap radial flux permanent magnet vernier machine with yokeless rotor,” Energies, vol. 14, no. 8,pp. 2311, Apr. 2021. DOI:10.3390/en14082311.

[6] Z. Liu, W. Zhao, J. Ji and Q. Chen, "Electromagnetic performance of double-stator flux-modulation permanent-magnet motor," IEEE Transactions on Applied Superconductivity, vol. 26, no. 4, pp. 1-5, Art no. 5205205, Jun. 2016. DOI: 10.1109/TASC.2016.2544101.

[7] A. Mousaei, M. B. Bannae Sharifian and N. Rostami, "Direct Thrust Force Control (DTFC) of Optimized Linear Induction Motor with Super Twisting Sliding Mode Controller (STSMC)," 2021 12th Power Electronics, Drive Systems, and Technologies Conference (PEDSTC), 2021, pp. 1-5, doi: 10.1109/PEDSTC52094.2021.9405903.

[8] Y. Gao, R. Qu, D. Li, J. Li and G. Zhou, “Design of a dual-stator LTS vernier machine for direct-drive wind power generation,” IEEE Transactions on Applied Superconductivity, vol. 26, no. 4, pp. 1–5, Art ID: 5204505, Jun. 2016. DOI:10.1109/TASC.2016.2540610.

[9] Y. Gao, D. Li , R. Qu and H. Ding, “A double-stator flux switching PM machine with multi-PM MMF harmonics,” IEEE Transactions on Magnetics, vol. 55, no. 6, pp. 1–6, Art ID: 8202206, Jun. 2019. DOI: 10.1109/TMAG.2019.2903838.

[10] X. Zhu, M. Cheng, X. Li and Y. Wang, “Topology analysis, design, and comparison of high temperature superconducting double stator machine with stationary seal,” IEEE Transactions on Applied Superconductivity, vol. 30, no. 1, pp. 1–10, Art ID: 5200110, Jan. 2020. DOI: 10.1109/TASC.2019.2914041.

[11] Arash Mousaei, Nasim Bahari, Guo Mieho. Artificial Neural Networks (ANN) of Proposed Linear Induction Motor with Hybrid Secondary (HLIM) Considering the End Effect. American Journal of Electrical and Computer Engineering. Vol. 5, No. 1, 2021, pp. 32-39. doi: 10.11648/j.ajece.20210501.15.

[12] Y. Li, D. Bobba and B. Sarlioglu, “A novel 6/4 flux-switching permanent magnet machine designed for high-speed operations,” IEEE Transactions on Magnetics, vol. 52, no. 8, pp. 1–9, Art ID: 8107109, Aug. 2016. DOI: 10.1109/TMAG.2016.2547366.

[13] Ocak, C., “Design, Analysis and Application of a New Three Level Brushless DC Motor for Electric Vehicles”, Ph. D. Thesis, Graduate School of Natural and Applied Sciences, Gazi University, Ankara, 2013.

[14] S. Asgari, R. Yazdanpanah and M. Mirsalim, “A dual-stator machine with diametrically magnetized PM: analytical air-gap flux calculation, efficiency optimization, and comparison with conventional dual-stator machines,” Scientia Iranica D, vol. 29, no. 1, pp. 208–216, 2022. DOI: 10.24200/sci.2019.53316.3181.

[15] A. Mousaei, M. B. Bannae Sharifian and N. Rostami, "An Improved Predictive Current Control Strategy of Linear Induction Motor Based on Ultra-Local Model and Extended State Observer," 2022 13th Power Electronics, Drive Systems, and Technologies Conference (PEDSTC), 2022, pp. 12-18, doi: 10.1109/PEDSTC53976.2022.9767535.

[16] Y. Fan, G. Qu, C. Tan, Q. Zhang and W. Wang, “Design and analysis of a new five-phase dual-stator consequent-pole brushless hybrid excitation machine,” IEEE Transactions on Magnetics, vol. 55, no. 1, pp. 1–10, Art ID: 8100410, Jan. 2019. DOI: 10.1109/TMAG.2018.2878982.

[17] Y. Zhao, W. Huang, W. Jiang, X. Lin and X. Wu, “Optimal design and performance analysis of dual-stator permanent magnet fault-tolerant machine,” IEEE Transactions on Magnetics, vol. 57, no. 2, pp. 1–6, Art ID: 8102906, Feb. 2021. DOI: 10.1109/TMAG.2020.3026327.

[18] A. Mousaei, M. B. Bannae Sharifian and N. Rostami, "An Improved Fuzzy Logic Control Strategy of an Optimized Linear Induction Motor Using Super Twisting Sliding Mode Controller," 2022 13th Power Electronics, Drive Systems, and Technologies Conference (PEDSTC), 2022, pp. 1-5, doi: 10.1109/PEDSTC53976.2022.9767465.

[19] Z.Q. Zhu and J.T. Chen, "Advanced flux-switching permanent magnet brushless machines," IEEE Transactions on Magnetics, vol. 46, no. 6, pp. 1447–1453, Jun. 2010. doi: 10.1109/TMAG.2010.2044481.

[20] Z.Q. Zhu and X. Liu, "Individual and global optimization of switched flux permanent magnet motors," Proceedings of IEEE International Conference on Electrical Machines and Systems, Beijing, China, Aug. 2011, pp. 1–6. DOI:10.1109/ICEMS.2011.6073806.